

Research



**Cite this article:** Majerová M, Klement R, Prnová A, Kraxner J, Bruneel E, Galusek D. 2018 Crystallization and visible–near-infrared luminescence of Bi-doped gehlenite glass. *R. Soc. open sci.* **5**: 181667.  
<http://dx.doi.org/10.1098/rsos.181667>

Received: 1 October 2018

Accepted: 6 November 2018

**Subject Category:**

Chemistry

**Subject Areas:**

materials science

**Keywords:**

gehlenite, flame synthesis, glass microspheres, photoluminescence properties, Bi<sup>3+</sup>-doped glasses

**Author for correspondence:**

M. Majerová

e-mail: melinda.majerova@savba.sk

This article has been edited by the Royal Society of Chemistry, including the commissioning, peer review process and editorial aspects up to the point of acceptance.



# Crystallization and visible–near-infrared luminescence of Bi-doped gehlenite glass

M. Majerová<sup>1</sup>, R. Klement<sup>2</sup>, A. Prnová<sup>3</sup>, J. Kraxner<sup>2</sup>, E. Bruneel<sup>4</sup> and D. Galusek<sup>2,3</sup>

<sup>1</sup>Department of Magnetometry, Institute of Measurement Science, Slovak Academy of Sciences, Dúbravská cesta 9, SK-842 19 Bratislava, Slovak Republic

<sup>2</sup>Centre for Functional and Surface Functionalized glass, Alexander Dubček University of Trenčín, Študentská 2, SK-911 50 Trenčín, Slovak Republic

<sup>3</sup>Vitrum Laugaricio – Joint Glass Center of the IIC SAS, TnU AD and FCHPT STU, Študentská 2, SK-911 50 Trenčín, Slovak Republic

<sup>4</sup>Department of Chemistry, Ghent University, Krijgslaan 281 S3, Gent 9000, Belgium

ORCID iD MM, 0000-0002-5054-5135; AP, 0000-0002-1713-3171

Gehlenite glass microspheres, doped with a different concentration of Bi<sup>3+</sup> ions (0.5, 1, 3 mol%), were prepared by a combination of solid-state reaction followed by flame synthesis. The prepared glass microspheres were characterized from the point of view of surface morphology, phase composition, thermal and photoluminescence (PL) properties by optical and scanning electron microscopy (SEM), X-ray diffraction (XRD), differential scanning calorimetry (DSC) and PL spectroscopy. The closer inspection of glass microsphere surface by SEM confirmed a smooth surface. This was further verified by XRD. The basic thermal characteristics of prepared glasses, i.e.  $T_g$  (glass transition temperature),  $T_x$  (onset of crystallization peak temperature),  $T_i$  (temperature of the inflection point of the crystallization peak) and  $T_p$  (maximum of crystallization peak temperature), were estimated from the DSC records. High-temperature XRD experiments in the temperature interval range 600–1100°C were also performed. The PL emission properties of prepared glasses and their polycrystalline analogues (glass crystallized at 1000°C for 10 h) were studied in the visible and near-infrared (NIR) spectral range. When excited at 300 nm, the glasses, as well as their polycrystalline analogues, exhibit broad emission in the visible spectral range from 350 to 650 nm centred at about 410–450 nm, corresponding to Bi<sup>3+</sup> luminescence centres. The emission intensity of polycrystalline samples was found to be at least 30 times higher than the emission of their glass analogues. In addition, a weak emission band was observed around 775 nm under 300 nm excitation. This band was attributed to the presence of a minor amount of Bi<sup>2+</sup> species in prepared samples. In the NIR spectral range, the broad band emission was observed in the spectral range of

1200–1600 nm with the maxima at 1350 nm. The chemistry of Bi and its oxidation state equilibrium in glasses and polycrystalline matrices is discussed in detail.

## 1. Introduction

Since the 1990s, compounds with melilite structure have been intensively studied due to their interesting electrochemical [1], magnetic [2–4], luminescence [5–7] and structural properties [8–10]. The melilites are a large family of materials with the general formula  $[^8]A_2[^4]B[^4]C_2O_7$  where A is a large cation such as Ca, Sr, Ba, Na, K, Y, lanthanides, Pb or Bi; B is a small cation such as Al, Be, Co, Cu, Cd, Fe, Ga or Mg; and finally C = Si, B, Al, Cr, Ge or V. The number in square brackets [N] indicates the coordination number (CN) of the element. The structure of melilite compounds, which belong to a sorosilicate group of minerals, was first determined by Warren [11]. The structure has a tetragonal symmetry space group P-4<sub>2</sub>m and consists of BC<sub>2</sub>O<sub>7</sub> layers parallel to (0 0 1) with corner-sharing BO<sub>4</sub> and CO<sub>4</sub> tetrahedra. The A cations are placed between these layers in distorted square antiprisms of oxygen atoms. Owing to their tetragonal and non-centrosymmetric crystal structure, lanthanides or transition metals can be accepted as dopants by the melilites [3].

Rare earth ion-doped melilite-type materials represented by gehlenite (Ca<sub>2</sub>Al<sub>2</sub>SiO<sub>7</sub>) have been intensively investigated over the past few decades. For example, gehlenite doped with Nd<sup>3+</sup> ions is a good candidate for diode pumped laser, with a broad absorption around 806 nm [12]. Ca<sub>2</sub>Al<sub>2</sub>SiO<sub>7</sub>:Eu<sup>3+</sup>, Tb<sup>3+</sup> as a potential candidate for phosphor converted light-emitting diodes was reported by Yang *et al.* [13]. Bernardo *et al.* compared amorphous Eu<sup>3+</sup>-doped gehlenite-based glass phosphor materials with their polycrystalline analogues [6]. It was determined that amorphous phosphor materials allow for more homogeneous dopant (or activator) distribution, due to the lack of grain boundaries to segregate and accumulate the dopants.

Recently, the optical properties of Bi-doped oxide glasses have been intensively investigated [14,15]. These glasses have interesting properties, such as simple colouring [16], third-order optical nonlinearity [17] and luminescence in the ultraviolet–visible wavelength range [18]. Compared to rare-earth-doped glasses, Bi-doped glasses exhibit ultra-broad infrared emission in the wavelength region from 1000 to 1700 nm with a full width at half maximum of the emission band up to about 300 nm. The bismuth-doped glasses, crystals and fibres thus have the potential to become the next generation of ultra-broadband optical amplifiers [19–28]. In materials (including glasses), Bi ions can be present in four oxidation states: Bi<sup>+</sup>, Bi<sup>2+</sup>, Bi<sup>3+</sup> and Bi<sup>5+</sup>. As the melting temperature of the Bi-doped glasses increases, the bismuth valence state changes as follows:



where Bi<sub>2</sub>, Bi<sub>2</sub><sup>−</sup>, Bi<sub>3</sub>, etc. are Bi clusters and (Bi)<sub>n</sub> represents metallic colloidal particles. The melting temperature, the glass composition, the atmosphere and the concentration of other polyvalent elements all strongly affect the reaction sequence [29].

The nature of active centres emitting in the near infrared (NIR) range is still controversial. Several hypotheses have been proposed, which can be summarized into three groups. The NIR luminescence is attributed alternatively to the presence of (i) bismuth with higher valence (Bi<sup>5+</sup> and Bi<sup>5+</sup>O<sub>n</sub><sup>2+</sup> molecules) [23,30]; (ii) bismuth with lower valence (Bi<sup>+</sup>, neutral and negatively charged dimers—Bi<sub>2</sub>, Bi<sub>2</sub><sup>−</sup>, Bi<sub>2</sub><sup>2−</sup>) [20,31], the di- or tri-valent Bi ions are excluded, because it is generally known that Bi<sup>2+</sup> and Bi<sup>3+</sup> ions emit visible luminescence [15,18,32–34]; and (iii) point defects. To add to the confusion, changes of Bi activated NIR luminescence have been reported with the change of their local coordination. This indicates that NIR emission may be the result of the local structure of the active centres [14,23,35–37].

In this work, we investigated the luminescence properties of Bi<sub>2</sub>O<sub>3</sub>-doped gehlenite glass microspheres prepared by flame synthesis and studied the influence of crystallization of the glass on the luminescence in visible and NIR wavelength range.

## 2. Material and methods

Powder precursors for flame synthesis were prepared by solid-state reaction, from high-purity SiO<sub>2</sub> (p.a., Polske odczynniki chemiczne, Gliwice), Al<sub>2</sub>O<sub>3</sub> (p.a., Centralchem, Bratislava), Bi<sub>2</sub>O<sub>3</sub> (99.9%, STREM

Chemicals, USA) and  $\text{CaCO}_3$  (p.a., Centralchem, Bratislava). The compositions of prepared systems are summarized in table 1. At first, suitable amounts of the starting powders were weighed and homogenized in an agate mill in isopropyl alcohol for 4 h. After drying under an infrared lamp, the powders were calcined in a two-step process at  $1000^\circ\text{C}$  for 4 h in air. In the next step, the calcined powders were annealed at  $1300^\circ\text{C}$  for 4 h in a Pt crucible.

Glass microspheres were prepared from powder precursors by flame synthesis. The powders were fed into  $\text{CH}_4\text{--O}_2$  flame with an estimated temperature of about  $2800^\circ\text{C}$ . The molten particles were quenched by spraying them with distilled water (to achieve a sufficient cooling rate to avoid crystallization), separated and dried. To eliminate any residual carbon from flame synthesis, the glass microspheres were calcined for 4 h at  $650^\circ\text{C}$  in air.

Primary information on the morphology of prepared microspheres was obtained by optical microscopy (Nikon ECLIPSE ME 600) in transmitted light at  $10\text{--}50\times$  magnification. More detailed examination of prepared glass microspheres was carried out by scanning electron microscopy (FEG SEM JEOL 7600F) at an accelerating voltage of 20 kV. The microspheres were fixed on an aluminium sample holder using conductive adhesive graphite tape and sputtered with gold (Carl Zeiss SC 7620 sputter coater) to prevent charging. For the SEM examination of a polished cross section of glass microspheres, the microspheres were embedded into a polymeric resin (Simplimet 1000, Buehler), carefully polished to prepare cross sections (Ecomet 300, Buehler) and sputtered with carbon to prevent charging.

The differential scanning calorimetry (DSC) measurements were carried out in the temperature range ( $30\text{--}1200^\circ\text{C}$ ) with the use of Netzsch STA 449 F1 Jupiter analyser. Nitrogen atmosphere (5.0 purity), heating rate ( $10^\circ\text{C min}^{-1}$ ) and platinum crucibles with the sample mass  $\approx 15$  mg were used in the DSC experiments.

Phase compositions of prepared precursor powders and glass microspheres were studied by powder X-ray diffraction (XRD; Panalytical Empyrean,  $\text{CuK}\alpha$  radiation, at ambient temperature in the  $2\theta$  range of  $10\text{--}80^\circ$ ). The crystallization properties of prepared microspheres were investigated by high-temperature XRD (HT XRD) using the same diffractometer equipped with a high-temperature cell (Anton Paar HTK 16), in the temperature range  $600\text{--}1100^\circ\text{C}$  in ambient atmosphere, and a heating rate of  $10^\circ\text{C min}^{-1}$ . The software High Score Plus (v. 3.0.4, Pananalytical, The Netherlands) was used to evaluate diffraction data with the use of the COD 2017 database.

The photoluminescence spectra were recorded using Fluorolog FL3-21 spectrometer (Horiba Jobin Yvon) with Xe (450 W) arc lamp as an excitation source. The luminescence properties of Bi-doped gehlenite glasses were compared with their crystalline analogues obtained by isothermal crystallization of glass at  $1000^\circ\text{C}$  for 10 h under ambient atmosphere.

### 3. Results and discussion

Preliminary inspection of prepared glasses using optical microscopy revealed that the glass particles were of spherical shape and were transparent in the visible wavelength region (figure 1*a*). Their diameter varied between 2 and  $20\text{ }\mu\text{m}$  with a mean value of  $\approx 7\text{ }\mu\text{m}$  similar for all prepared compositions. The representative particle size distribution is shown in figure 1*b*, with the predominant fraction of beads having a diameter in the range of 4 to  $10\text{ }\mu\text{m}$ . More detailed examination of prepared glass microbeads was carried out by SEM. Representative SEM micrographs of microspheres are shown in figure 1*c,d*. Amorphous nature of glass microspheres was indicated by their smooth surfaces. SEM examination of polished cross sections confirmed the amorphous character of prepared glass microspheres; no morphological features indicating the presence of crystalline phases (e.g. facets, second phase inclusions) were observed (figure 1*d*).

The phase composition of prepared glass microspheres was identified using XRD, as shown in the inset of figure 2. The absence of any discrete diffraction maxima and the presence of a broad band in the  $2\theta$  range  $24^\circ\text{--}36^\circ$  in XRD patterns of all prepared compositions confirmed their amorphous nature. The XRD patterns of microspheres crystallized at  $1000^\circ\text{C}$  for 10 h (figure 2) confirmed their polycrystalline character with the presence of pure gehlenite (01-074-1607 COD) as the only crystalline phase.

Thermal properties of the prepared glasses were studied using DSC. DSC study of glass microspheres revealed significant differences in thermal behaviour of prepared systems. The DSC record of GBi0.5 sample contained one relatively broad exothermic peak centred at  $996^\circ\text{C}$ , which is close to the peak temperature of pure gehlenite glass prepared as microspheres,  $T_p$  approximately  $994^\circ\text{C}$  (figure 3). This exothermic effect was attributed to the crystallization of the gehlenite phase. Similar values around approximately  $1000^\circ\text{C}$  were also reported for gehlenite glass prepared by melt-quenching technique [38,39]. As the

**Table 1.** Composition and temperature parameters of investigated glasses from DSC at 10°C min<sup>−1</sup>;  $T_g$ —glass transition temperature,  $T_x$ —crystallization onset temperature,  $T_f$ —temperatures of the inflection points of the crystallization peak,  $T_p$ —peak temperature of crystallization.

sample	composition (mol.%)				XRD quality	mean diameter (μm)	$T_g$ (°C)	$T_x$ (°C)	$T_f$ (°C)	$T_{f2}$ (°C)	$T_p$ (°C)
	CaO	Al <sub>2</sub> O <sub>3</sub>	SiO <sub>2</sub>	Bi <sub>2</sub> O <sub>3</sub>							
GBi0.0	50.00	25.00	25.00	0.0	amorphous	n.d.	860	970	980	996	994
GBi0.5	49.76	24.87	24.87	0.5	amorphous	7.1	863	978	989	1003	996
GBi1.0	49.50	24.75	24.75	1.0	amorphous	7.3	860	944	962	992	976
GBi3.0	48.50	24.25	24.25	3.0	amorphous	7.4	837	867	874	892	884
							938	938	961	990	973

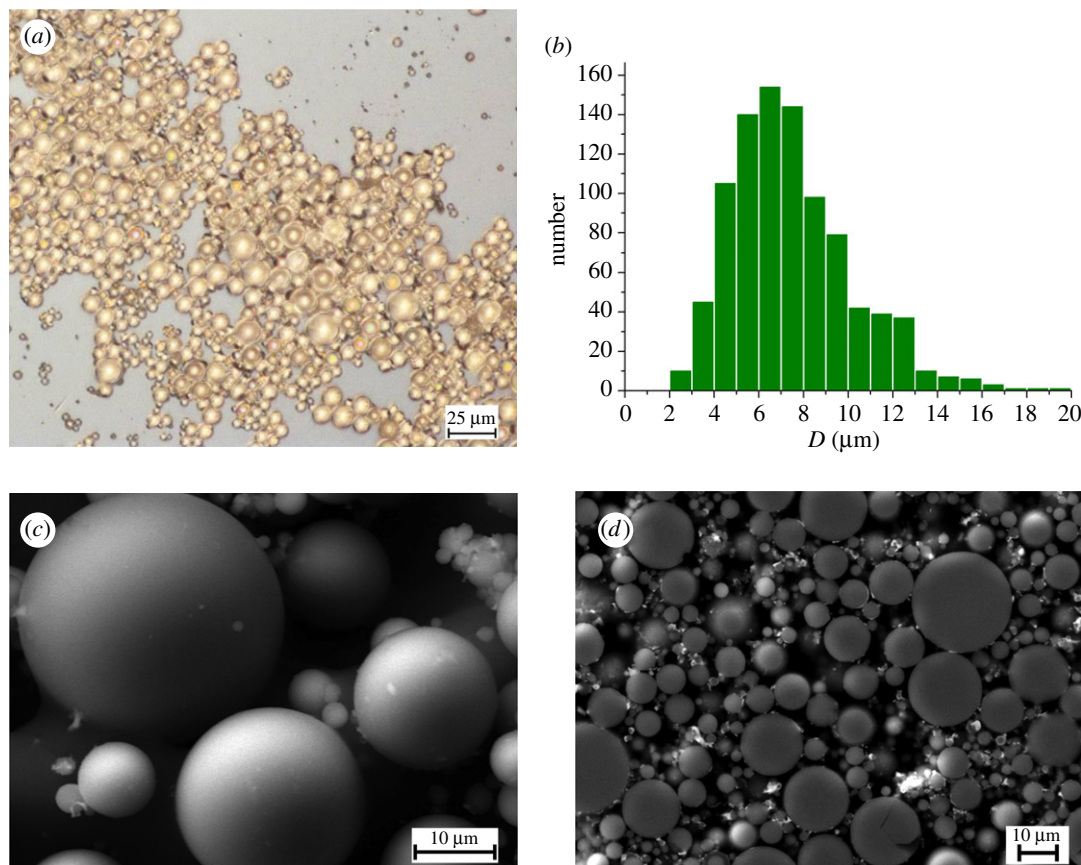


**Figure 1.** The results of optical microscopy and SEM examination and particle size distribution of prepared microspheres. (a) Optical micrograph of GBi0.5 microspheres, (b) particle size distribution of GBi3.0, (c) SEM image of as-prepared GBi3.0 microspheres, (d) SEM micrograph of a polished cross section of the GBi3.0 sample.

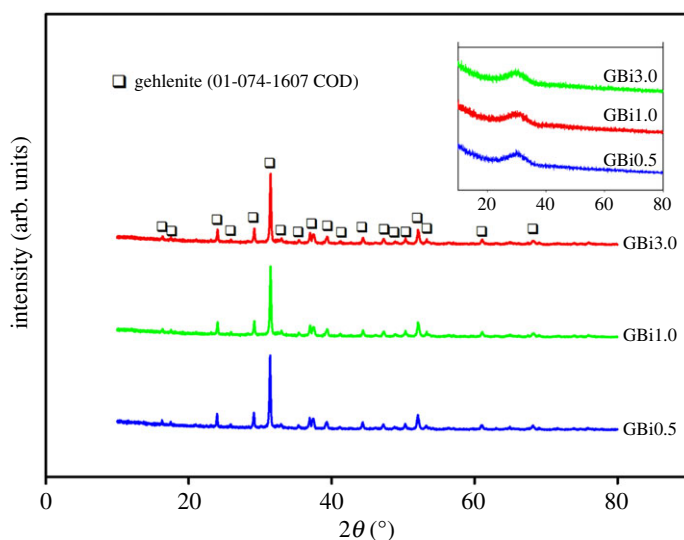


**Figure 2.** XRD patterns of crystallized microspheres (1000°C/10 h). The inset shows XRD patterns of Bi-doped gehlenite glassy particles after flame synthesis.

concentration of  $\text{Bi}_2\text{O}_3$  in glass increases, the peak temperature is significantly shifted (about 20°C) to lower temperatures and broadened. For the sample GBi1.0, the DSC record contained one broad exothermic peak centred at 976°C; however, also the indication of another exothermic effect with the maxima at around 930°C was observed in the DSC trace. On the contrary, the DSC curve of GBi3.0 sample contained two broad exothermic peaks centred at 884°C and 973°C (figure 3), respectively.



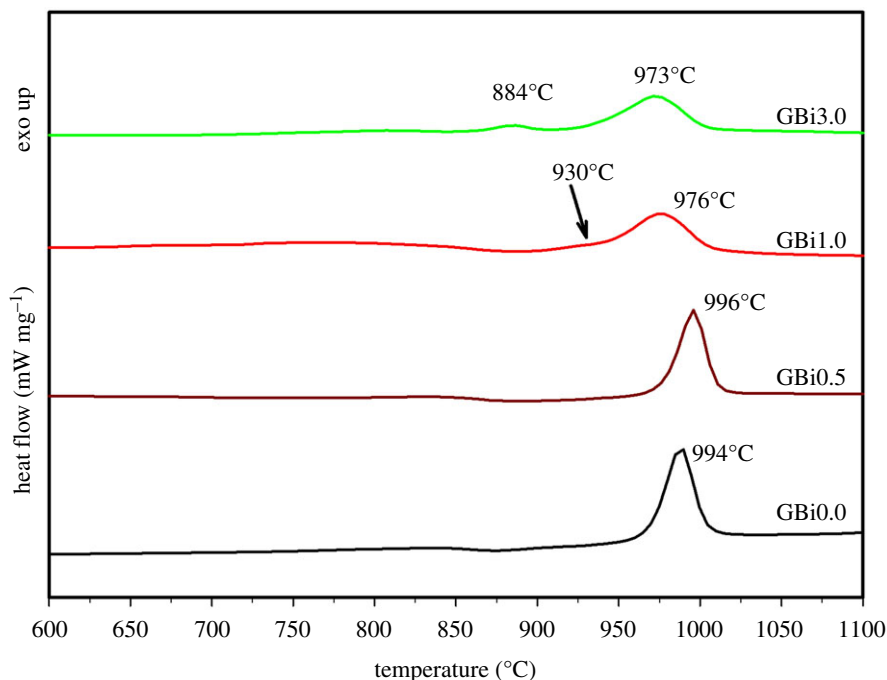


**Figure 3.** DSC records of prepared Bi-doped gehlenite glass microspheres.

The glass transition temperature ( $T_g$ ) and the onset of crystallization temperature ( $T_x$ ) were also estimated from the DSC records. In addition, the inflection points of crystallization peaks ( $T_{f1}$ ,  $T_{f2}$ ) were determined (the first derivatives of the DSC curves). The basic thermal characteristics of prepared glasses are summarized in table 1. The temperatures  $T_g$ ,  $T_x$  and  $T_p$  are shifted towards lower values with the increase in bismuth content in glass (table 1). As reported by Reddy *et al.* [40] in a study of melilite-type glasses with the addition of  $\text{Bi}_2\text{O}_3$ , the increase in  $\text{Bi}_2\text{O}_3$  content may give rise to a decrease in the Si–O–Si bridging oxygen of the silicate structural units with progressive formation of non-bridging oxygens. This gradual depolymerization of the glass network well explains the observed decrease in  $T_g$  values from 863°C to 837°C. The lower values of  $T_x$  and  $T_p$  indicate the higher tendency of GBi1.0 and GBi3.0 glasses to crystallization in comparison with the GBi0.5. As  $\text{Bi}_2\text{O}_3$  plays the role of network modifier [41], the increased tendency towards crystallization is most likely due to a decrease in viscosity of the glasses (partially depolymerized glass network), which may facilitate diffusion of cations. The decrease in  $T_g$  and  $T_p$  values with increasing  $\text{Bi}_2\text{O}_3$  content was also reported by Kim *et al.* [41] for the glasses in the system  $\text{Bi}_2\text{O}_3$ – $\text{B}_2\text{O}_3$ – $\text{SiO}_2$ . Moreover,  $\text{Bi}_2\text{O}_3$  may act as an effective nucleating agent, thus leading to the decrease in nucleation/crystallization temperature and unusual thermal behaviour of GBi1.0 and GBi3.0 glasses. The crystallization process, however, seems to be more complex and further detailed kinetic study is required.

To determine the origin of the first peak in the DSC record of GBi3.0 glass and to better understand thermal behaviour of prepared samples, HT XRD experiments were performed and phase evolution with temperature was studied. HT XRD experiments were carried out in the temperature interval 600–1100°C, at the heating rate of 5°C min<sup>−1</sup>, and with an XRD pattern recorded every 10°C. Figure 4 shows selected diffraction patterns measured during the non-isothermal HT XRD experiments. Crystallization of only gehlenite phase (01-074-1607 COD) was observed in the whole measured temperature interval, with the onset of crystallization at 800°C for GBi3.0 sample, 870°C for GBi1.0 and 920°C for GBi0.5. These temperatures correspond to the temperature at which the most intense peak of the gehlenite phase ( $\langle 1, 2, 1 \rangle$ ) was first observed in the XRD trace and raised. The results obtained are in good agreement with the results of DSC analysis. From the diffraction patterns recorded at different temperatures, the temperature dependences of the relative intensity of the most intense gehlenite peak at  $2\theta = 31.394^\circ$  were determined (figure 5) and temperature intervals with the most pronounced increase in relative intensity of the  $\langle 1, 2, 1 \rangle$  gehlenite peak were estimated. These were found to be as follows: (800–820)°C and (930–940)°C for the GBi3.0 glass, (960–970)°C for GBi1.0, and (940–950)°C for GBi0.5. The presence of two temperature intervals with the highest increase in relative intensity of the  $\langle 1, 2, 1 \rangle$  gehlenite peak in GBi3.0 corresponds to the presence of two peaks in DSC record and suggests crystallization of

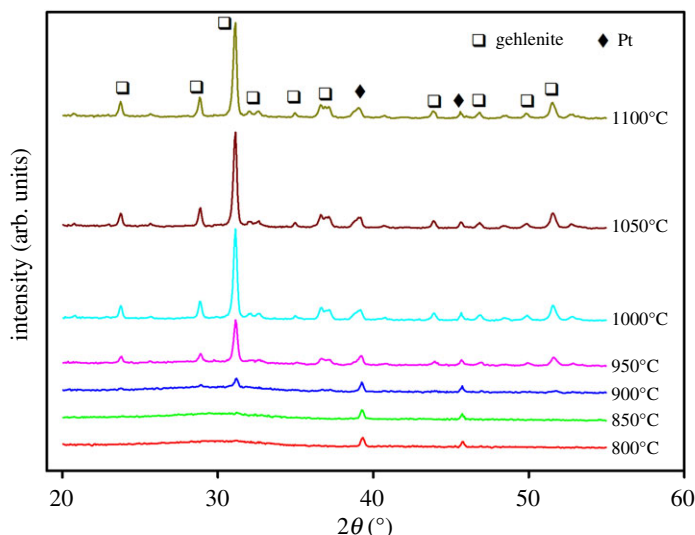


**Figure 4.** HT XRD records of the GBi3.0 microspheres recorded at various temperatures.

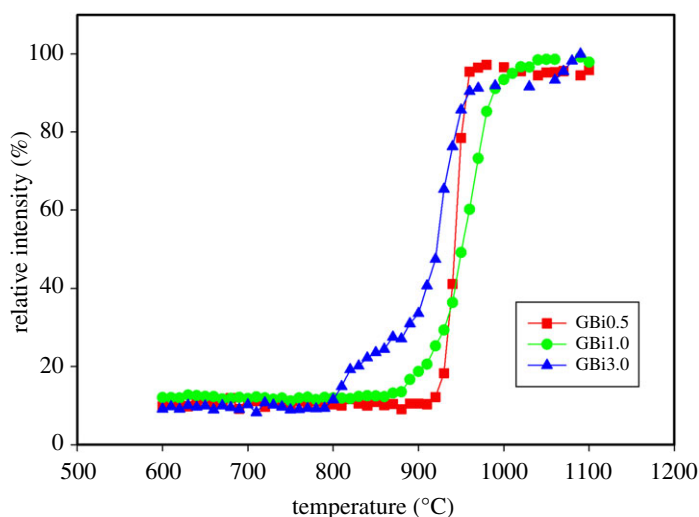


**Figure 5.** Temperature dependences of relative intensities of the  $\langle 1, 2, 1 \rangle$  gehlenite diffraction peak.

gehlenite phase in two steps. Figure 6 also indicates that the crystallization of GBi0.5 glass is completed at temperature  $\approx 990^\circ\text{C}$ , and for GBi1.0 and GBi3.0 glasses at approximately  $1040^\circ\text{C}$ . Above this temperature only negligible growth of relative intensity of the  $\langle 1, 2, 1 \rangle$  gehlenite peak was observed.

Based on the non-isothermal HT XRD and DSC analysis, an isothermal HT XRD experiment was performed with the GBi3.0 glass. The glass microspheres were heated to  $884^\circ\text{C}$  and one XRD pattern was recorded every 5 min with a total duration of isothermal heating of 240 min. The results of this experiment showed crystallization of only one phase—gehlenite (01-074-1607 COD). Time dependence of the relative content of gehlenite phase in isothermally annealed GBi3.0 sample is shown in figure 6. After a fast initial increase in the content of crystalline gehlenite in the first 20 min, the crystallization slowed down, and the content of crystalline gehlenite increases approximately linearly until the end of the experiment.

The photoluminescence (PL) emission properties of prepared glasses and crystalline analogues (glass crystallized at  $1000^\circ\text{C}$  for 10 h) were studied in the visible and NIR spectral range. The excitation and emission spectra of prepared samples are shown in figure 7. Owing to the very low PL emission intensity of glasses compared to the polycrystalline samples, the discussion is mainly focused on the PL properties of polycrystalline samples.

The  $\text{Bi}^{3+}$  ion has  $6s^2$  electron configuration and thus the ground state is  $^1S_0$ , and  $6s6p$  configuration in the excited state, which gives rise to the triplet levels  $^3P_0$ ,  $^3P_1$ ,  $^3P_2$  and singlet state  $^1P_1$ , in order of increasing energy. According to the dipole selection rules, excitations usually occur from the  $^1S_0$

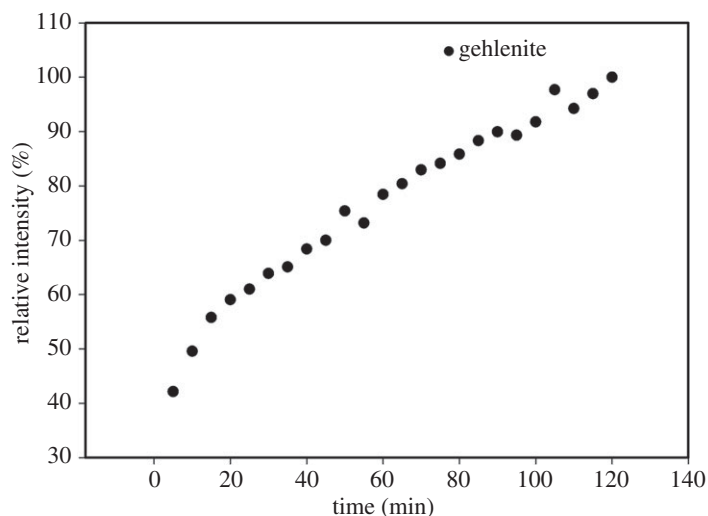


**Figure 6.** The time dependence of the relative intensity of the  $\langle 1, 2, 1 \rangle$  gehlenite peak during isothermal heating at  $884^{\circ}\text{C}$ .

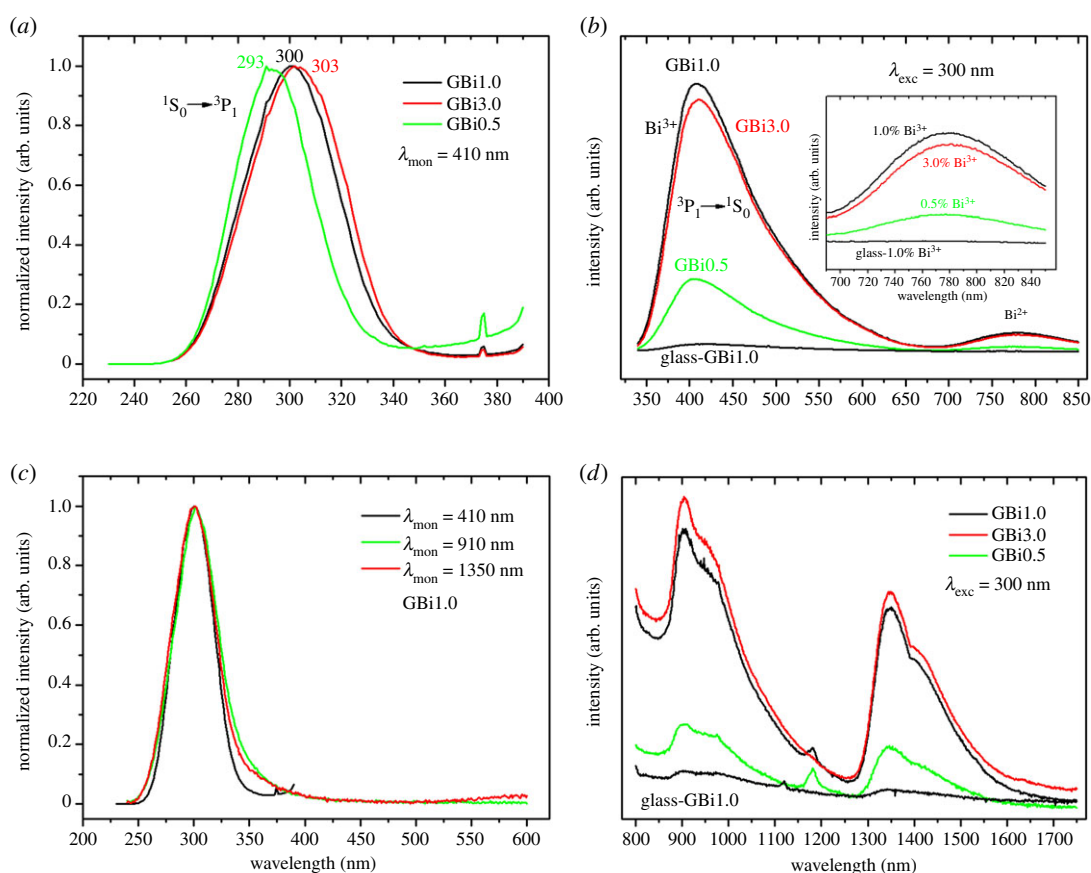


**Figure 7.** The photoluminescence excitation (*a,c*) and emission spectra (*b,d*) of  $\text{Bi}^{3+}$ -doped crystallized microspheres.

ground state to the  $^3\text{P}_1$  and  $^1\text{P}_1$  states [42]. The excitation spectra ( $\lambda_{\text{mon}} = 410 \text{ nm}$ ) exhibit broad absorption band centred at about  $300 \text{ nm}$ , corresponding to  $^1\text{S}_0 \rightarrow ^1\text{P}_1$  transition of  $\text{Bi}^{3+}$ , that is slightly red shifted as the concentration of  $\text{Bi}^{3+}$  ions increases (from  $293$  to  $303 \text{ nm}$ ); figure 7*a*. When excited at  $300 \text{ nm}$ , the glasses as well as their crystalline analogues exhibit broad emission band in the visible spectral range from  $350$  to  $650 \text{ nm}$  centred at about  $410\text{--}450 \text{ nm}$ , corresponding to  $^3\text{P}_1 \rightarrow ^1\text{S}_0$  transition within the  $\text{Bi}^{3+}$  luminescence centres. Similar broadband emission was observed by Li *et al.* [5] in charge non-compensated and alkali ion charge compensated  $\text{Bi}^{3+}$  doped gehlenite, obtained by solid-state reaction. The blue emission intensity of crystalline samples is high and was found to be at



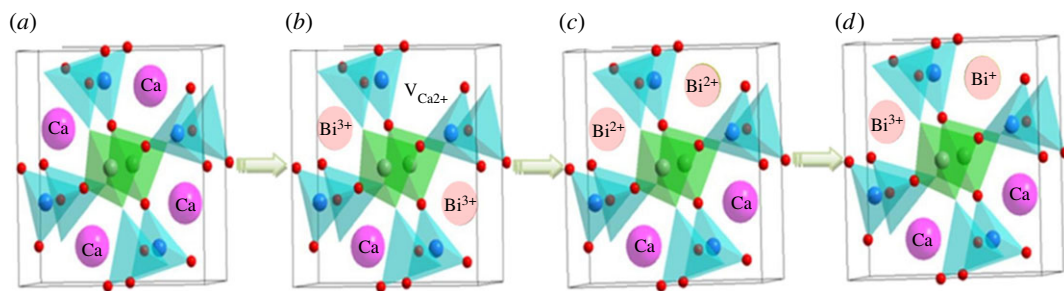


**Figure 8.** (a) The  $\text{Ca}_2\text{Al}_2\text{SiO}_7$  host structure; (b) the incorporation of the  $\text{Bi}^{3+}$  ions; (c,d) the incorporation of the  $\text{Bi}^{2+}$  ions; the incorporation of the  $\text{Bi}^{3+}$  and  $\text{Bi}^{+}$  ions into the host structure for charge compensation [5].

least 30 times higher than the emission of the glass samples with colour coordinates at  $(x, y = 0.196, 0.191)$ . The PL intensity increases with increasing  $\text{Bi}^{3+}$  concentration. However, for sample with 3% of  $\text{Bi}^{3+}$ , the intensity is lowered thus indicating that concentration quenching may operate at this doping level.

In addition, a weak emission band was observed around 775 nm under 300 nm light excitation. This band is due to the presence of  $\text{Bi}^{2+}$  species in prepared samples. The electron configuration of  $\text{Bi}^{2+}$  is  $6s^2 6p^1$  with  $^2P_{1/2}$  ground state and  $^2P_{3/2}$  as the first excited state. This excited state can be further separated by crystal field splitting into two sublevels  $^2P_{3/2}(1)$  and  $^2P_{3/2}(2)$ , in order of increasing energy. In fact, the transition  $^2P_{3/2}(1) \rightarrow ^2P_{1/2}$  is responsible for emission that is usually observed in the orange–red spectral range (emission maxima 600–700 nm) [43]. The shift of this emission found in our Bi-doped samples to the deep red spectral range indicates the strong crystal field splitting of the  $^2P_{3/2}$  states.

In the NIR spectral region, two broad band emissions were observed in the spectral ranges of 850–1200 and 1200–1600 nm with the maxima at 905 and 1350 nm, respectively (figure 7c,d). The first emission is superposed on the deep red emission originating from  $^2P_{3/2}(1) \rightarrow ^2P_{1/2}$  transition of  $\text{Bi}^{2+}$  ions. The concentration dependence of NIR emission intensity follows the same order as described above for visible range emission. The origin of these NIR emissions is still a matter of dispute; however, many authors ascribe this transition to the lower oxidation state of the bismuth, such as  $\text{Bi}^{+}$ ,  $\text{Bi}^0$  or cluster ions [44]. Thus, it is reasonable to expect that the observed NIR emissions originate from  $\text{Bi}^{+}$  ions incorporated in the gehlenite crystal host.

The structure of gehlenite ( $\text{Ca}_2\text{Al}_2\text{SiO}_7$ ) is schematically depicted in figure 8a. The Ca atoms are closely surrounded by  $(\text{Al/Si})\text{O}_7$  and  $\text{AlO}_4$  polyhedra creating a porous structure.  $\text{Ca}^{2+}$  in the tetragonal  $\text{Ca}_2\text{Al}_2\text{SiO}_7$  is coordinated with eight  $\text{O}^{2-}$  atoms, forming a distorted polyhedron. When  $\text{Bi}^{3+}$  is doped into  $\text{Ca}_2\text{Al}_2\text{SiO}_7$ , it tends to substitute for calcium rather than aluminium or silicon sites as a result of matched ionic size (note that for  $\text{Bi}^{3+}$  with CN of 8,  $R_{\text{Bi}^{3+}, \text{CN}=8} = 1.17 \text{ \AA}$ ; and  $R_{\text{Ca}^{2+}, \text{CN}=8} = 1.12 \text{ \AA}$ ;  $R_{\text{Al}^{3+}, \text{CN}=4} = 0.39 \text{ \AA}$ ;  $R_{\text{Si}^{4+}, \text{CN}=4} = 0.26 \text{ \AA}$ ). There is, however, a charge imbalance between  $\text{Bi}^{3+}$  and  $\text{Ca}^{2+}$  ions. In general, the charge imbalance is induced by creation of internal defects, for instance, negatively charged  $\text{Ca}^{2+}$  vacancies or positively charged  $\text{O}^{2-}$  vacancies. These internal structural defects often lead to quenching of luminescence due to the energy transfer from luminescence centres to defects. Figure 8b demonstrates such a situation, when  $3\text{Ca}^{2+}$  ions have been replaced by  $2\text{Bi}^{3+}$  ions, resulting in a  $\text{Ca}^{2+}$  vacancy:  $3\text{Ca}^{2+} = 2\text{Bi}^{3+} + \text{V}_{\text{Ca}^{2+}}$ . In order to compensate the charge defect, the  $\text{M}^{+}$  ion (e.g. alkali ions  $\text{Li}^{+}$ ,  $\text{Na}^{+}$ ,  $\text{K}^{+}$ ) should be introduced as the charge compensation or the  $\text{Bi}^{3+}$  ion should change its oxidation state to  $\text{Bi}^{2+}$  and/or  $\text{Bi}^{+}$  (figure 8c,d). This is most likely the case in samples studied in this work, as documented by PL emissions originating from three different bismuth sites,  $\text{Bi}^{3+}$ ,  $\text{Bi}^{2+}$  and  $\text{Bi}^{+}$ , respectively. All three bismuth oxidation states were also observed in PL spectra of the prepared glass samples, however, with much lower emission intensity.

## 4. Conclusion

Three Bi-doped gehlenite precursor powders with different content of  $\text{Bi}_2\text{O}_3$  (0.5, 1, 3 mol%) were prepared by a standard solid-state reaction method. X-ray amorphous glass microspheres, with diameters up to  $25 \mu\text{m}$  and transparent in visible light, were then prepared from the precursor powders by flame synthesis. The addition of various amounts of Bi has a significant effect on the thermal properties of prepared glass microspheres:

1. For the compositions with the lowest Bi content, only one exothermic effect was observed corresponding to the crystallization of gehlenite phase. In the case of a sample containing 1.0 mol% of  $\text{Bi}_2\text{O}_3$ , the DSC record contains one broad exothermic peak but with an indication of another exothermic effect. Two exothermic maxima were found on the DSC curve of the GeBi3.0 glass.
2. The glass transition temperature and the onset of crystallization temperature of gehlenite glasses decrease with increasing content of Bi in the samples.
3. The HT XRD results confirmed the crystallization of gehlenite over the entire temperature range indicating that it was a two-step gehlenite crystallization in the case of GBi3.0 glass. The crystallization mechanism of gehlenite phase in GBi1.0 and GBi3.0 glasses is not a trivial one and detailed study of crystallization kinetics is required to clarify this effect.

The PL emission properties of prepared glasses and their crystalline analogues (glass crystallized at  $1000^\circ\text{C}$  for 10 h) were studied in the visible and NIR spectral range. The emission intensity of crystalline samples was found to be at least 30 times higher than the emission of the glass analogues. The three types of PL emissions in different spectral regions (visible, deep red and NIR range) revealed the simultaneous presence of bismuth ions in three oxidation states  $\text{Bi}^{3+}$ ,  $\text{Bi}^{2+}$  and  $\text{Bi}^+$ , with the last two oxidation states stabilizing the host structure and compensating charge imbalance between the  $\text{Bi}^{3+}$  and  $\text{Ca}^{2+}$  ions. This structural arrangement favours replacement of  $\text{Ca}^{2+}$  in the crystal host and, hence, strong luminescence emission from  $\text{Bi}^{3+}$ .

Data accessibility. All data are included in the paper.

Authors' contributions. M.M., J.K. and E.B. carried out the preparation of the precursor powders and glasses via flame-spraying synthesis, crystallization experiments and SEM microscopy of samples; M.M. also drafted the manuscript. A.P. completed DSC analysis and data interpretation. D.G. carried out the XRD and HT XRD measurements, phase analysis, interpretation of the data and gave suggestions on the writing of the whole manuscript. R.K. conducted the photoluminescence measurements and data interpretation and drafted the manuscript. All authors gave final approval for publication.

Competing interests. We declare we have no competing interests.

Funding. This paper is a part of dissemination activities of the project FunGlass. This project has received funding from the European Union's Horizon 2020 research and innovation programme under grant agreement no. 739566. This work was supported by VEGA 1/0527/18, APVV-17-0049 and VEGA 2/0164/17.

## References

1. Park HJ, Kim TG, Kwak C, Lee S, Lee KH. 2015  $\text{Sr}_2(\text{Mg}_{1-x}\text{Ga}_x)\text{Ge}_2\text{O}_7+0.5x$ : melilite-type oxygen ionic conductor associated with fivefold coordinated germanium and gallium. *J. Power Sources* **275**, 884–887. (doi:10.1016/j.jpowsour.2014.11.088)
2. Nöller R, Knoll H. 1983 Magnetic properties of calcium-silicates (diopside and gehlenite) doped with iron (III). *Solid State Commun.* **47**, 237–239. (doi:10.1016/0038-1098(83)90552-5)
3. Yahia HB, Essehlri R, Belharouak I, Gaudin E. 2015 Crystal structure and magnetic properties of  $\text{K}_2\text{CoV}_2\text{O}_7$ . *Mater. Res. Bull.* **71**, 7–10. (doi:10.1016/j.materresbull.2015.06.038)
4. Majerova M, Dvureckenskij A, Cigan A, Skratek M, Pmova A, Kraxner J, Galusek D, Manka J. 2017 Magnetic properties of synthetic gehlenite glass microspheres. *Acta Phys. Pol. A* **131**, 699–701. (doi:10.12693/APhysPolA.131.699)
5. Li M, Wang L, Ran W, Liu Q, Ren Ch, Jiang H, Shi J. 2016 Broadly tuning emission from  $\text{Ca}_2\text{Al}_2\text{SiO}_7$ :Bi phosphor based on crystal field modulation around Bi ions. *New J. Chem.* **40**, 9579–9585. (doi:10.1039/C6NJ01755J)
6. Bernardo E, Fiocco L, Pmova A, Klement R, Galusek D. 2014 Gehlenite:Eu3+ phosphors from a silicone resin and nano-sized. *Opt. Mater.* **36**, 1243–1249. (doi:10.1016/j.optmat.2014.03.007)
7. Shih SJ, Lin YCH, Lin SH, Vetska P, Galusek D, Tuan WH. 2016 Preparation and characterization of Eu-doped gehlenite glassy particles using spray pyrolysis. *Ceram. Int.* **42**, 11 324–11 329. (doi:10.1016/j.ceramint.2016.04.053)
8. Florian P, Veron E, Green TFG, Yates JR, Massiot D. 2012 Elucidation of the Al/Si ordering in gehlenite  $\text{Ca}_2\text{Al}_2\text{SiO}_7$  by combined  $^{29}\text{Si}$  and  $^{27}\text{Al}$  NMR spectroscopy/quantum chemical calculations. *Chem. Mater.* **24**, 4068–4079. (doi:10.1021/cm3016935)
9. Teixeira VC, Montes PJR, Valerio MEG. 2014 Structural and optical characterization of  $\text{Ca}_2\text{Al}_2\text{SiO}_7$ : $\text{Ce}^{3+}$ ,  $\text{Mn}^{2+}$  nanoparticles produced via a hybrid route. *Opt. Mater.* **36**, 1580–1590. (doi:10.1016/j.optmat.2014.04.037)
10. Luo Y, Xia Z. 2014 Effect of partial nitridation on the structure and luminescence properties of melilite-type  $\text{Ca}_2\text{Al}_2\text{SiO}_7$ : $\text{Eu}^{2+}$  phosphor. *Opt. Mater.* **36**, 1874–1876. (doi:10.1016/j.optmat.2014.03.032)
11. Warren BE. 1930 The structure of melilite  $(\text{Ca},\text{Na})_2(\text{Mg},\text{Al})(\text{Si},\text{Al})_2\text{O}_7$ . *Z. Kristallogr.* **75**, 131–138.
12. Viana B, Lejus AM, Saber D, Duxin N, Vivien D. 1994 Optical properties and energy transfer among  $\text{Nd}^{3+}$  in  $\text{Nd}:\text{Ca}_2\text{Al}_2\text{SiO}_7$  crystals for diode pumped lasers. *Opt. Mater.* **3**, 307–316. (doi:10.1016/0925-3467(94)90043-4)
13. Yang P et al. 2013  $\text{Ca}_2\text{Al}_2\text{SiO}_7$ : $\text{Bi}^{3+}$ ,  $\text{Eu}^{3+}$ ,  $\text{Tb}^{3+}$ : a potential single-phased tunable-color-emitting phosphor. *J. Lumin.* **135**, 206–210. (doi:10.1016/j.jlumin.2012.10.015)
14. Liu JF. 2015 Luminescence properties of bismuth-doped  $\text{SrO-B}_2\text{O}_3$  glasses with multiple valences state. *Optik* **126**, 4115–4118. (doi:10.1016/j.jlloe.2015.07.207)
15. Peng M, Wondraczek L. 2009  $\text{Bi}^{2+}$ -doped strontium borates for white-light-emitting diodes. *Opt. Lett.* **34**, 2885–2887. (doi:10.1364/OL.34.002885)
16. Weyl WA. 1999 *Coloured glasses*. Sheffield, UK: Society of Glass Technology.
17. Lin G, Tan D, Luo F, Chen D, Zhao Q, Qiu J. 2011 Linear and nonlinear optical properties of glasses doped with Bi nanoparticles. *J. Non-Cryst. Solids* **357**, 2312–2315. (doi:10.1016/j.jnoncrsol.2010.11.052)
18. Xu W, Peng M, Ma Z, Dong G, Qiu J. 2012 A new study on bismuth doped oxide glasses.

- Opt. Express* **20**, 15692–15702. (doi:10.1364/OE.20.015692)
19. Denker BI, Galagan BI, Sverchkov SE, Dianov EM. 2013 Short-lifetime near-infrared emission centers in bismuth-doped oxide glasses. *Laser Phys.* **23**, 105803. (doi:10.1088/1054-660X/23/10/105803)
  20. Ren J, Qiu J, Chen D, Hu X, Jiang X, Zhu C. 2008 Luminescence properties of bismuth-doped lime silicate glasses. *J. Alloys Compd.* **463**, L5–L8. (doi:10.1016/j.jallcom.2007.09.026)
  21. Qiu J, Peng M, Ren J, Meng X, Jiang X, Zhu C. 2008 Novel Bi-doped glasses for broadband optical amplification. *J. Non-Cryst. Solids* **354**, 1235–1239. (doi:10.1016/j.jnoncrsol.2007.02.094)
  22. Dianov EM, 2010 On the nature of near-IR emitting Bi centres in glass. *Quantum Electron.* **40**, 283–285. (doi:10.1070/QE2010v04n04ABEH014304)
  23. Fujimoto Y. 2010 Local structure of the infrared bismuth luminescent center in bismuth-doped silica glass. *J. Am. Ceram. Soc.* **93**, 581–589. (doi:10.1111/j.1551-2916.2009.03419.x)
  24. Meng XG, Qiu JR, Peng MY, Chen DP, Zhao QZ, Jiang XW, Zhu CS. 2005 Near infrared broadband emission of bismuth-doped aluminophosphate glass. *Opt. Express* **13**, 1628–1634. (doi:10.1364/OPEX.13.001628)
  25. Fujimoto Y, Nakatsuka M. 2001 Infrared luminescence from bismuth-doped silica glass. *Jpn. J. Appl. Phys.* **40**, 279–281.
  26. Peng M, Chen D, Qiu J, Jiang X, Zhu C. 2007 Bismuth-doped zinc aluminosilicate glasses and glass-ceramics with ultra-broadband infrared luminescence. *Opt. Mater.* **29**, 556–561. (doi:10.1016/j.optmat.2005.08.049)
  27. Peng M, Zollfrank C, Wondraczek L. 2009 Origin of broad NIR photoluminescence in bismuthate glass and Bi-doped glasses at room temperature. *J. Phys. Condens. Matter* **21**, 285106. (doi:10.1088/0953-8984/21/28/285106)
  28. Nielsen KH, Smedskjaer MM, Peng M, Yue Y, Wondraczek L. 2012 Surface-luminescence from thermally reduced bismuth-doped sodiumaluminosilicate glasses. *J. Non-Cryst. Solids* **358**, 3193–3199. (doi:10.1016/j.jnoncrsol.2012.09.021)
  29. Khonthon S, Morimoto S, Arai Y, Ohishi Y. 2009 Redox equilibrium and NIR luminescence of Bi<sub>2</sub>O<sub>3</sub>-containing glasses. *Opt. Mater.* **31**, 1262–1268. (doi:10.1016/j.optmat.2009.01.005)
  30. Kustov EF, Bulatov LI, Dvoyrin VV, Mashinsky VM. 2009 Molecular orbital model of optical centers in bismuth-doped glasses. *Opt. Lett.* **34**, 1549–1551. (doi:10.1364/OL.34.001549)
  31. Peng M, Qiu J, Chen D, Meng X, Zhu C. 2005 Superbroadband 1310 nm emission from bismuth and tantalum codoped germanium oxide glasses. *Opt. Lett.* **30**, 2433–2435. (doi:10.1364/OL.30.002433)
  32. Reisfeld R, Boehm L. 1974 Optical properties of bismuth in germinate, borax and phosphate glasses. *J. Non-Cryst. Solids* **16**, 83–92. (doi:10.1016/0022-3093(74)90070-2)
  33. Oomen EWJL, Blasse G. 1988 Luminescence of Bi<sup>3+</sup> in the metaphosphates LnP<sub>3</sub>O<sub>9</sub> (Ln = Sc, Lu, Y, Gd, La). *J. Solid State Chem.* **75**, 201–204. (doi:10.1016/0022-4596(88)90318-0)
  34. Hamstra MA, Folkerts HF, Blasse G. 1994 Red bismuth emission in alkaline-earth-metal sulfates. *J. Mater. Chem.* **4**, 1349–1350. (doi:10.1039/JM9940401349)
  35. Ohkura T, Fujimoto Y, Nakatsuka M, Young-Seok S. 2007 Local structures of bismuth ion in bismuth-doped silica glasses analyzed using Bi L<sub>III</sub> X-ray absorption fine structure. *J. Am. Ceram. Soc.* **90**, 3596–3600. (doi:10.1111/j.1551-2916.2007.01934.x)
  36. He X, Xu X, Yan C, Qiu J. 2015 Local structure regulating effect for the near infrared luminescence of Bi in zinc silicate and germanate glasses. *Optik* **126**, 3624–6327. (doi:10.1016/j.ijleo.2015.08.242)
  37. Wang L, Moon BK, Choi BCH, Kim JH, Shi J, Jeong JH. 2016 Photoluminescent properties and site occupation preference in Bi<sup>3+</sup>, Eu<sup>3+</sup> doped CaY<sub>4</sub>(SiO<sub>4</sub>)<sub>3</sub>O phosphor. *Ceram. Int.* **42**, 12971–12980. (doi:10.1016/j.ceramint.2016.05.070)
  38. Orsini PG, Buri A, Marotta A. 1975 Devitrification of glasses in the akermanite-gehlenite system. *J. Am. Ceram. Soc.* **58**, 306–311.
  39. Marotta A, Buri A, Valenti G.L. 1978 Crystallization kinetics of Gehlenite glass. *J. Mater. Sci.* **13**, 2483–2486.
  40. Reddy AA, Tulyaganov DU, Kappor S, Goel A, Pascual MJ, Kharton VV, Ferreira JMF. 2012 Study of melilite based glasses and glass-ceramics nucleated by Bi<sub>2</sub>O<sub>3</sub> for functional applications. *RSC Adv.* **2**, 10 955–10 967. (doi:10.1039/C2RA22001F)
  41. Kim BS, Lim ES, Lee JH, Kim JJ. 2006 Effect of Bi<sub>2</sub>O<sub>3</sub> content on sintering and crystallization behavior of low-temperature firing Bi<sub>2</sub>O<sub>3</sub>-B<sub>2</sub>O<sub>3</sub>-SiO<sub>2</sub> glasses. *J. Eur. Ceram. Soc.* **27**, 819–824. (doi:10.1016/j.jeurceramsoc.2006.04.013)
  42. Yousif A, Jafer RM, Som S, Duvenhage MM, Coetsee E, Swart HC. 2015 Ultra-broadband luminescent from a Bi doped CaO matrix. *RSC Adv.* **5**, 54115–54122. (doi:10.1039/C5RA09246A)
  43. Peng M, Wondraczek L. 2010 Orange-to-red emission from Bi<sup>2+</sup> and alkaline earth codoped strontium borate phosphors for white light emitting diodes. *J. Am. Ceram. Soc.* **93**, 1437–1442. (doi:10.1111/j.1551-2916.2009.03590.x)
  44. Peng M, Dong G, Wondraczek L, Zhang L, Zhang N, Qiu J. 2011 Discussion on the origin of NIR emission from Bi-doped materials. *J. Non-Cryst. Solids* **357**, 2241–2245. (doi:10.1016/j.jnoncrsol.2010.11.086)